Remote Sensing of Cirrus Cloud Particle Size and Optical Depth Using Polarimetric Sensor Measurements

S. C. OU, K. N. LIOU, AND Y. TAKANO

Department of Atmospheric and Oceanic Sciences, University of California, Los Angeles, Los Angeles, California

R. L. SLONAKER

Raytheon ITSS Corp., Upper Marlboro, Maryland

(Manuscript received 30 August 2004, in final form 20 May 2005)

ABSTRACT

This paper presents a conceptual approach toward the remote sensing of cirrus cloud particle size and optical depth using the degree of polarization and polarized reflectance associated with the first three Stokes parameters, I, Q, and U, for the 0.865- and 2.25-μm wavelengths. A vector line-by-line equivalent radiative transfer program including the full Stokes parameters based on the adding method was developed. The retrieval algorithm employs the steepest-descent method in the form of a series of numerical iteration procedures to search for the simulated polarization parameters that best match the measured values. Sensitivity studies were performed to investigate the behavior of phase-matrix elements as functions of scattering angles for three ice crystal size–shape combinations. Overall, each phase-matrix element shows some sensitivity toward ice crystal shape, size, and surface roughness due to the various optical effects. Synthetic analysis reveals that the retrieval algorithm is highly accurate, while polarimetric and radiometric error sources cause very small retrieval errors. Finally, an illustrative example of applying the retrieval algorithm to airborne Polarization and Directionality of the Earth's Reflectances (POLDER) data during the European Cloud and Radiation Experiment (EUCREX) is presented.

1. Introduction

The importance of cirrus clouds in weather and climate processes has been recognized as a result of numerous observational and modeling studies (Liou 2002; Mace et al. 1997; Wylie and Menzel 1999; Lynch et al. 2002). Several approaches to the satellite remote sensing of cirrus cloud particle size distribution using solar reflectance measured by space-borne multispectral radiometers have been developed (Minnis et al. 1998; King et al. 1997; Ou et al. 1999; Rolland et al. 2000). These techniques exploit the spectral dependence of the ice extinction of atmospheric radiation, using radiometric measurements for visible and near-infrared wavelengths at which absorption by water vapor and other gases is minimal (the window bands), and at which the scattering and absorption by cloud particles are sensitive to ice crystal size distribution. While initial success has been claimed by the radiometric approaches, the accuracy of their application to remote sensing data suffers from the uncertainty in surface reflectivity (Rolland and Liou 2001) and ice crystal shape (Rolland et al. 2000; Mishchenko et al. 1996). Retrievals combining polarimetric together with radiometric measurements, which include a derived parameter, the degree of polarization, may produce more accurate cirrus cloud information, because this parameter has a high measurement accuracy on the order of 0.2% (Cairns et al. 1999).

To explore the potential applicability of cirrus cloud remote sensing using polarimetric sensor data, Takano and Liou (1989a,b) and Liou and Takano (1994) used the single-scattering properties for hexagonal plates and columns, and later a combination of regular and irregular ice particles to interpret the measured linear polarization pattern of sunlight reflected from optically thick cirrus clouds presented by Coffeen (1979). Liou and Takano (2002) demonstrated that information regarding ice crystal shape and orientation can be in-

Corresponding author address: Dr. Szu-Cheng Ou, Department of Atmospheric and Oceanic Sciences, University of California, Los Angeles, 405 Hilgard Ave., Los Angeles, CA 90095-1565.
E-mail: ssou@atmos.ucla.edu

ferred from the reflected polarization patterns based on comprehensive theoretical interpretations. The remote sensing of cirrus clouds using the Polarization and Directionality of the Earth's Reflectances (POLDER) polarized radiance data has been reported by Chepfer et al. (1998, 1999a,b). Sauvage et al. (1999) analyzed airborne POLDER 0.864-μm measurements from cirrus clouds during the European Cloud and Radiation Experiment (EUCREX) 1994 campaign and derived optimal ice crystal shape models that best fit the polarization data. Masuda et al. (2002) developed an algorithm for retrieving cirrus cloud optical thickness and ice crystal shape using space-borne POLDER polarized reflectance data.

In this paper, we present a conceptual approach for the remote sensing of cirrus cloud particle size and optical depth using the degree of polarization and three polarized reflectances for the 0.865- and 2.25-μm spectral bands measured at multiple viewing angles. In general, visible reflectances are more sensitive to cloud optical thickness, while near- and shortwave-infrared (IR) reflectances are more sensitive to ice crystal size (King et al. 1997; Liou 2002; Ou et al. 1999, 2003; Rolland et al. 2000). Radiative transfer simulations confirm this behavior, since polarized reflectances for 2.25 μm exhibit more sensitivity to cloud particle size than those for 0.865 μm (as shown in Fig. 3b). In addition, both bands are in the spectral window regions, and the 2.25-μm observations are less sensitive to Rayleigh and aerosol scattering contributions than the 0.865-μm band. For these reasons, we have included the 2.25-μm polarized reflectance in the present program to enhance the retrieval accuracy of cloud particle size. Applicable 0.865- and 2.25-μm observations are currently available from the Research Scanning Polarimeter (RSP; Cairns et al. 1999) and are planned for the Aerosol Polarimetric Sensor (APS), which will be on board the National Aeronautics and Space Administration (NASA) Glory mission scheduled to be launched in December 2007. A vector line-by-line equivalent (VLBLE) radiative transfer program based on the principle of the adding method has been developed for the computation of polarized radiative transfer involving ice crystals in cirrus clouds to interpret the polarization pattern observed from space and to assist in the development of remote sensing algorithms.

The present approach differs from the methodologies developed by a number of POLDER scientists. First, it utilizes one visible channel and one near-IR channel, whereas Chepfer et al. (1999a,b) and Masuda et al. (2002) used only one visible channel. Second, our approach infers both cirrus cloud optical depth and ice crystal mean effective size, whereas Chepfer et al. (1999a,b) retrieved only ice crystal shape and Masuda et al. (2002) inferred ice crystal shape and optical depth. Third, our approach employs four polarization parameters, whereas the previous methods used at most two polarization parameters. Finally, our approach can be applied to data from an along-track scanning polarimeter with the availability of pixels scanned multiple times at different angles, whereas the previous methods have been largely applied to POLDER datasets that are composed of single-scan pixels.

This paper is organized as follows. In section 2, we present the theoretical basis for the VLBLE along with the determination of single-scattering parameters and phase-matrix elements. We also describe the solution procedure for the retrieval algorithm. In section 3, we show results of the sensitivity study including the behavior of the phase-matrix elements as functions of the scattering angle, variation in the polarization parameter with the viewing angle, verification of the retrieval algorithm by synthetic studies, and an example illustrating the potential applicability of the present retrieval algorithm to airborne POLDER data and the like. Concluding remarks are given in section 4.

2. Theoretical description of a conceptual retrieval approach

a. Formulation and modeling of radiative transfer involving polarization

A reliable and accurate radiative transfer program is needed for the purpose of developing a cloud remote sensing algorithm and performing a sensitivity study. In this study, we follow the radiative transfer scheme developed by Takano and Liou (1989a,b) for vertically inhomogeneous atmospheres based on the adding method including the full set of Stokes parameters. The general equation governing the transfer of diffuse Stokes vector denoted by $\mathbf{I} = [I, Q, U, V]$ can be written in the form (Liou 2002)

$$\mu \frac{d\mathbf{I}(\tau; \mu, \phi)}{d\tau} = \mathbf{I}(\tau; \mu, \phi) - \mathbf{J}(\tau; \mu, \phi), \tag{1}$$

where $\mu = \cos\theta$, θ is the viewing zenith angle, ϕ is the relative azimuthal angle, τ is the optical depth, and the source function is given by

$$\mathbf{J}(\tau; \mu, \phi) = \frac{\varpi}{4\pi} \int_0^{2\pi} \int_{-1}^{1} \mathbf{Z}(\mu, \phi; \mu', \phi')\mathbf{I}(\tau; \mu', \phi')\, d\mu'\, d\phi' + \frac{\varpi}{4\pi}\mathbf{Z}(\mu, \phi; -\mu_0, \phi_0)\pi\mathbf{F}_0 \exp(-\tau/\mu_0), \tag{2}$$

where ϖ is the single-scattering albedo, $\mathbf{F}_0$ represents the Stokes vector for the incident solar irradiance, $\mu_0 = \cos\theta_0$, θ_0, and ϕ_0 are the solar zenith and solar azimuthal angles, respectively, where the negative sign of $-\mu_0$ denotes the downward direction of the incident solar radiation. Here $\mathbf{Z}$ is the phase matrix defined with respect to the local meridian plane as follows:

$$\mathbf{Z}(\mu, \phi; \mu', \phi') = \mathbf{L}(\pi - i_2)\mathbf{P}(\Theta)\mathbf{L}(-i_1), \tag{3}$$

where $\mathbf{L}$ is the transformation matrix required to rotate the meridian plane containing the incident and outgoing vectors to the scattering plane (Hovenier 1969), and i_1 and i_2 denotes the angles between the meridian planes containing incident and scattered vectors and the scattering plane, respectively.

To apply the doubling principle for radiative transfer to the solution of the multiple-scattering problem involving polarization, we first define the bidirectional reflection matrix $\mathbf{R}(\mu, \phi, \mu', \phi')$ and transmission matrix $\mathbf{T}(\mu, \phi, \mu', \phi')$ for the light beam incident from above a cloud layer. The reflected and transmitted Stokes parameter vectors for this incident light beam can be expressed in terms of the incident Stokes parameter vectors in the following forms:

$$\mathbf{I}_{\text{out, top}}(\mu, \phi) = \frac{1}{\pi}\int_0^{2\pi}\int_0^1 \mathbf{R}(\mu, \phi; \mu', \phi')\mathbf{I}_{\text{in, top}}(\mu', \phi')\mu'\, d\mu'\, d\phi', \tag{4}$$

$$\mathbf{I}_{\text{out, bottom}}(\mu, \phi) = \frac{1}{\pi}\int_0^{2\pi}\int_0^1 \mathbf{T}(\mu, \phi; \mu', \phi')\mathbf{I}_{\text{in, top}}(\mu', \phi')\mu'\, d\mu'\, d\phi'. \tag{5}$$

Likewise, we can also define the reflection matrix, $\mathbf{R}^*(\mu, \phi; \mu', \phi')$, and transmission matrix, $\mathbf{T}^*(\mu, \phi; \mu', \phi')$, for the light beam incident from below the cloud layer.

To proceed with the adding procedure, we start with an infinitesimal layer with an extremely small optical depth $\Delta\tau$ (e.g., 10^{-8}). Based on the single-scattering approximation, the reflection and transmission matrices for this differential layer can be expressed as follows:

$$\mathbf{R}(\mu, \phi; \mu', \phi') \approx \frac{\Delta\tau}{4\mu\mu'}\varpi\mathbf{Z}(-\mu, \phi; \mu', \phi'), \tag{6}$$

$$\mathbf{T}(\mu, \phi; \mu', \phi') \approx \frac{\Delta\tau}{4\mu\mu'}\varpi\mathbf{Z}(-\mu, \phi; -\mu', \phi'). \tag{7}$$

Equations (6) and (7) are similar to the initialization equations for scalar radiative transfer [Eqs. (6.4.8a) and 6.4.8b) in Liou 2002], except that the phase function term is replaced by the phase matrix, $\mathbf{Z}$ whose elements are expanded in the Fourier series with respect to the relative azimuthal angle. Each coefficient in the expansion is determined based on the orthogonality property of the Fourier components. Subsequently, the doubling procedure (Takano and Liou 1989a,b) is applied to the cloud layer to obtain the layer reflection and transmission matrices, and hence the reflected and transmitted Stokes parameters. The input parameters required to drive the VLBLE solar radiation model include the spectral wavenumber, solar and viewing zenith angles, relative azimuthal angle, spectral surface albedos, single-scattering parameters, and phase-matrix elements. The output polarization parameters are generated for selected ice crystal mean sizes, optical depths, and Gaussian angles.

b. *Single-scattering parameters and phase-matrix elements*

To simulate cirrus cloud scattering/absorption effects on radiative transfer, it is essential that reliable single-scattering parameters and phase-matrix elements as functions of the cloud particle shape and size distribution and scattering angle are precomputed for input in VLBLE. Single-scattering parameters include the extinction and scattering coefficients ($\beta_{e,s}$), the single-scattering albedo (ϖ), and the asymmetry factor (g). For a spectrum of randomly oriented hexagonal ice crystal sizes, the average extinction and scattering coefficients are obtained from (Takano and Liou 1989a,b)

$$\beta_{e,s} = \int_{L_1}^{L_2} C_{e,s}(L)n(L)\, dL, \tag{8}$$

where $C_{e,s}(L)$ is the extinction and scattering cross section, $n(L)$ is the ice crystal size distribution in terms of the maximum dimension L, with L_1 and L_2 being the lower and upper limits of L in the size distribution, respectively. The average single-scattering albedo is then parameterized as follows:

$$\varpi = \beta_s/\beta_e = \sum_{n=0}^{4}(-1)^n b_n z^n,$$

$$z = k_i\left(\frac{D}{2}\right)\frac{3\sqrt{3}(L/D)}{\sqrt{3} + 4(L/D)}, \tag{9}$$

and the average single-scattering albedo is defined by

$$\overline{\varpi} = \int_{L_1}^{L_2}\varpi C_e(L)n(L)\, dL \Big/ \int_{L_1}^{L_2} C_e(L)n(L)\, dL, \tag{10}$$

where D is the ice crystal width that is perpendicular to the maximum dimension L, and b_n are the empirical fitting coefficients given in Takano and Liou (1989a,b).

In general, the scattering phase matrix **P** consists of 16 elements and is a function of both the incoming (μ', ϕ') and outgoing (μ, ϕ) directions (Liou and Takano 2002). The expression for each nonzero element in terms of the four amplitude functions, S_j (j = 1–4) has been given by Takano and Liou (1993) for an ice crystal of arbitrary shape and size. Numerical results based on the geometric ray-tracing calculations reveal that the four elements in the upper-right and lower-left quadrants of the scattering phase matrix are all nearly zero, so that only eight elements remain to be determined. Furthermore, based on the law of reciprocity and symmetry considerations, the number of independent elements in the scattering phase matrix is reduced to six for ice particles randomly oriented in 3D space. In this case, the scattering phase matrix is given by

$$\mathbf{P} = \begin{bmatrix} P_{11} & P_{12} & 0 & 0 \\ P_{12} & P_{22} & 0 & 0 \\ 0 & 0 & P_{33} & -P_{43} \\ 0 & 0 & P_{43} & P_{44} \end{bmatrix}. \tag{11}$$

For nonspherical ice crystals, the phase function, P_{11}, contains a strong forward peak. The forward scattered energy within the scattering angle of 10° produced by the diffraction is about four to five orders of magnitude greater than that in the side and backscattered directions. To incorporate the forward peak contribution in multiple scattering, we consider an adjusted absorption and scattering atmosphere, such that the fraction of scattered energy residing in the forward peak is removed from the scattering parameters, which include the optical depth, the single-scattering albedo, and the asymmetry factor (Takano and Liou 1989a,b, 1995). For a spectrum of ice crystals defined by a size distribution $n(L)$, the phase-matrix elements can be obtained from

$$P_{ij}(\Theta) = \int_{L_1}^{L_2} P_{ij}(\Theta, L) C_s(L) n(L)\, dL \Big/ \int_{L_1}^{L_2} C_s(L) n(L)\, dL. \tag{12}$$

c. Retrieval algorithm

Polarimetric measurements are expressed in terms of the following fundamental parameters: the degree of polarization (P, also termed as the polarization ratio) and polarized reflectance for each measured Stokes parameter (r_I, r_Q, and r_U). These parameters are defined as follows:

$$P = \frac{\sqrt{Q^2 + U^2}}{I}, \tag{13}$$

$$r_I = \frac{\pi I}{\mu_0 F_0}, \tag{14}$$

$$r_Q = \frac{\pi Q}{\mu_0 F_0}, \tag{15}$$

$$r_U = \frac{\pi U}{\mu_0 F_0}, \tag{16}$$

where I, Q, and U are the Stokes parameters in W m^{-2} sr^{-1} μm^{-1}, μ_0 is the cosine of solar zenith angle, and F_0 is the spectral solar constant, which has the dimension of spectral flux. For 0.865- and 2.25-μm bands, F_0 = 986.23 and 77.18 W m^{-2} μm^{-1}, respectively. We have neglected the V component in our retrieval algorithm, because results of numerical computation show that its magnitude is always about three orders of magnitude smaller than the other three Stokes parameters.

The degree of polarization, P, is defined as a measure of the extent of polarization. Based on the design specification for the RSP, for example, the measured P exhibits an error of ~0.2% (Cairns et al. 1999) due to the cancellation of errors in radiometric calibration coefficients in I, Q, and U, which have about the same order of magnitude. Therefore, among the measured polarization parameters, the degree of polarization is most accurate. The polarized reflectances, r_I, r_Q, and r_U, are defined as the respective Stokes parameter multiplied by a factor of $\pi/\mu_0 F_0$. We note that the combination of r_Q and r_U in the form of $(r_Q^2 + r_U^2)^{1/2}$ has been used by Chepfer et al. (1998) for the interpretation of airborne POLDER polarization data over cirrus clouds. The factor μ_0 is added to normalize the polarized reflectance by the incident solar flux $\mu_0 F_0$. The π factor converts the dimension from flux to radiance, so that the polarized reflectance as it is defined is rendered dimensionless. Given that μ_0 and F_0 are accurately determined, the measured polarized reflectances will contain uncertainty of ~3%–5% due to the radiometric calibration error for individual Stokes components. These error sources are about an order of magnitude larger than that of P, but they are nonetheless useful in the remote sensing of cloud properties over inhomogeneous surfaces, as described in the following.

Both P and r_I are subject to the variation of surface albedo because of the inclusion of the intensity parameter, I, in the formulation of these parameters. Over

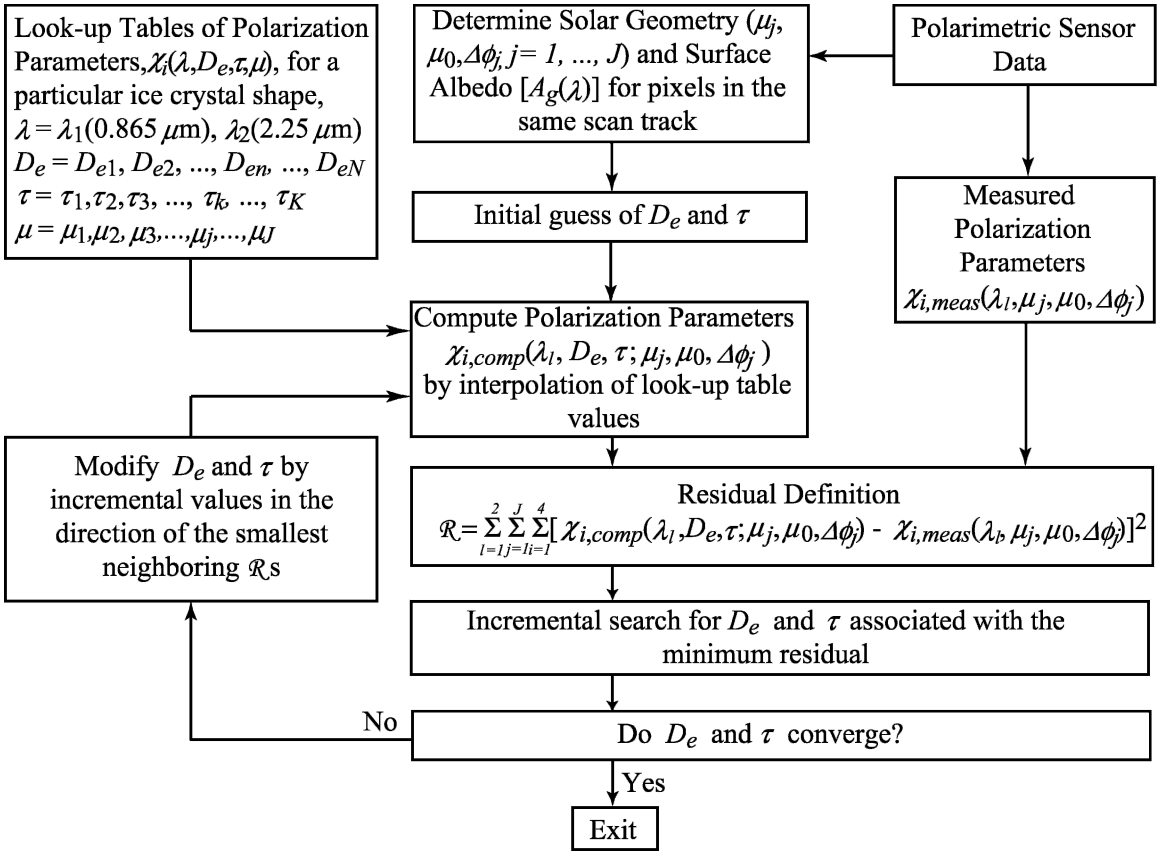

FIG. 1. Flowchart for the ice cloud retrieval algorithm. The parameter χ_i denotes a polarization parameter. It is the polarization ratio for $i = 1$, r_I for $i = 2$, r_Q for $i = 3$, and r_U for $i = 4$.

oceans, multiangle P values can be used to retrieve cloud properties with a reasonable accuracy due to the small variation in surface albedo. Over land, however, it would be difficult to use P values to retrieve optically thin cloud properties due to the spatial variation in surface type, which causes uncertainty in the prescription of surface albedo in the retrieval algorithm. As an alternative, r_Q and r_U can be used to improve the retrieval of cloud properties, because for thin cirrus clouds overlying a surface illuminated by the direct sunbeam, the contribution of polarized light reflected by the surface is negligible (Nadal and Bréon 1999; Goloub et al. 1994).

A schematic description of a multichannel multiparameter ice cloud retrieval algorithm is given as follows. This retrieval algorithm follows the principle of minimization of residuals in the multichannel correlation approach for the retrieval of cloud optical depth and mean particle size (King et al. 1997; Ou et al. 2003). Figure 1 shows the flowchart for retrieving ice crystal effective size and cloud optical depth. Lookup tables of polarization parameters are constructed before proceeding with the retrieval. For a particular ice crystal shape, we select three reference ice crystal mean effective sizes (24, 42, and 124 μm) and eight optical depths (0.125, 0.25, 0.5, 1, 2, 4, 8, and 16). Subsequently, we compute the polarization ratio (P) and polarized reflectances (r_I, r_Q, and r_U) for each combination of reference ice crystal mean effective size, optical depth, and the sensor channel and viewing geometry used for cloud retrieval.

In the retrieval program, we first prescribe the sun-sensor geometric parameters, including the solar zenith angle, the sensor-viewing zenith angle, and the relative azimuthal angle for each pixel. We also prescribe the surface albedo, which may be obtained from a histogram of clear reflectances or from the combination of the ecosystem map of surface types and spectral reflectivity library for various types of surface. Because the currently available polarimeters often scan a single spot multiple times at different viewing zenith angles, we may include J-scattering angle observations for each pixel in the retrieval algorithm. Thus, including 2 spectral bands and 4 polarization parameters, each pixel will

have $8 \times J$ pieces of observations for the solution of optical depth and ice crystal size.

The success of the retrieval algorithm would depend on the reliability of the determination of ice crystal shape or a mixture of shapes. In our analysis, although many shape factors in principle can be included, the angular distribution of polarized reflectances has been computed for the three basic ice crystal shapes that are assumed a priori. Thus, using these ice crystal models, the shape factor can be inferred based on multispectral and multiangle vector radiative transfer simulations (Liou and Takano 2002). The reliability of ice crystal shape determination from polarization remote sensing would be conditioned to independent validation, a subject requiring further research and development.

Among the four polarization parameters, only r_I, r_Q, and r_U are mutually independent, because P can be computed from these polarized reflectances. However, P is included due to its excellent measurement accuracy. Although there are $8 \times J$ observations, there exist correlations between the two spectral channels and among the J scattering angles. Certainly the number of independent observations is substantially less than $8 \times J$. As we are determining only two ice cloud properties, the solution remains overdetermined, and the retrieval problem is well posed. Because of compensation factors, all available pieces of information are to be used in the development of a remote sensing algorithm to enhance the retrieval accuracy. For example, the retrieval of cloud optical depth and particle size based on MODIS data utilizes both the 1.63- and 2.21-μm near-IR channels.

The retrieval algorithm employs the steepest-descent method (Tarantola 1987) in the form of a series of numerical iteration procedures to search for the computed polarization parameters that best match the measured polarization parameters. The steepest-descent method is an iterative numerical approach that systematically searches (in the direction of the largest decrease of the residual function) for the vector of unknowns that is associated with the residual minimum. The residual term is defined as

$$\mathcal{R} = \sum_{l=1}^{2} \sum_{j=1}^{J} \sum_{i=1}^{4} [\chi_{i,\,\mathrm{comp}}(\lambda_l, D_e, \tau; \mu_j, \mu_0, \Delta\phi_j) - \chi_{i,\,\mathrm{meas}}(\lambda_l, \mu_j, \mu_0, \Delta\phi_j)]^2, \quad (17)$$

where $\chi_{i,\mathrm{comp}}$ and $\chi_{i,\mathrm{meas}}$ are computed and measured polarization parameters, respectively.

We specify a first guess for the mean effective particle size ($D_e^{[0]}$) and optical depth ($\tau^{[0]}$). Thereafter, we use a three-dimensional linear interpolation scheme to compute the polarization parameters for the ice crystal mean effective size, optical depth, and viewing zenith angle based on entries in the precomputed lookup tables. We compute the residual functions for combinations of three cloud effective particle sizes ($D_e^{[0]} - \Delta D_e$, $D_e^{[0]}$, $D_e^{[0]} + \Delta D_e$), and three optical depths ($\tau^{[0]} - \Delta\tau$, $\tau^{[0]}$, $\tau^{[0]} + \Delta\tau$) with prescribed marching incremental ΔD_e and $\Delta\tau$. We then search for a new set of $D_e^{[1]}$ and $\tau^{[1]}$ that is associated with the smallest residual among the nine computed values. Subsequently, we repeat the computation of residuals for combinations of the three new cloud effective particle sizes ($D_e^{[1]} - \Delta D_e$, $D_e^{[1]}$, $D_e^{[1]} + \Delta D_e$) and three new optical depths ($\tau^{[1]} - \Delta\tau$, $\tau^{[1]}$, $\tau^{[1]} + \Delta\tau$). This process of the incremental search for the minimum-residual solution is repeated until successive values of ($D_e^{[n]}$, $\tau^{[n]}$) and ($D_e^{[n+1]}$, $\tau^{[n+1]}$) differ by less than a prescribed threshold value.

3. Sensitivity studies

The behavior of phase-matrix elements as functions of the scattering angle for different shapes of particles has been investigated by Cai and Liou (1982) who used the ray-tracing method to study the polarized light scattering by randomly oriented hexagonal column and plate ice crystals. Takano and Liou (1989a,b) used an improved ray-tracing program to compute phase-matrix elements for four size distributions consisting of randomly oriented hexagonal ice crystals and compared phase-matrix elements with available measurements. Polarized light scattering by ice crystals of polyhedral and irregular shapes has also been presented by Liou et al. (1983), Takano and Liou (1995), Yang and Liou (1998), Macke and Mishchenko (1996), and Yang and Cai (1991) for randomly oriented spheroids and finite circular cylinders.

Because of the complicated nature of the dependence of polarized parameters to ice crystal size and shape, we start from simulating the radiative transfer within clouds of uniform particle size and shape. Thus, we have chosen three sets of uniform size and shape: regular column with aspect ratio L/D = 120/60 (μm), irregular (rough surface) column with aspect ratio L/D = 120/60 (μm), and regular plate with aspect ratio L/D = 8/80 (μm), where L is the axial length (maximum dimension in the case of hexagonal column), and D is the diagonal width perpendicular to the axial length. Roughness of the irregular column is incorporated by randomly perturbing the normal of each crystal plane between 0° and 18°. The average perturbation angle is 9° and the azimuthal direction of each normal is also randomly distributed. Although we have only

prescribed the above three combinations, the scattering characteristics for other ice crystal shapes, sizes, and degrees of roughness can be approximated by one of these combinations. For example, the patterns of polarized light scattering by bullet rosettes and irregular aggregates can be approximated by using those of regular columns and ice particles with rough surfaces, respectively.

Ice crystals are assumed to be randomly oriented for the following reasons. Although Chepfer et al. (1999a) found that at least 40% of the POLDER data for ice clouds indicate the presence of horizontally oriented ice crystals, both Bréon and Dubrulle (2004) and Noel and Chepfer (2004) showed that the fraction of horizontally oriented ice crystals is normally small ($\sim 10^{-2}$). Liou and Takano (2002) have shown that by adding 0.1%–1.2% of horizontally oriented hollow column ice crystals, the subsun peaks in the measured angular distribution of polarized reflectances can be explained by radiative transfer simulations. Masuda et al. (2002) also assumed random orientation of ice crystals in their retrieval scheme of optical thickness and ice crystal shape using polarized reflectances from POLDER. Horizontally oriented crystals cause the polarized radiance to peak only in two directions: subsun ($\Theta = \pi - 2\theta_0$) and subanthelion ($\Theta = \pi$). Thus, the present retrieval algorithm would be applicable to all polarized radiance data, except those associated with these two specific angles.

a. Phase-matrix elements

Figure 2 shows the phase-matrix elements P_{11}, $-P_{12}/P_{11}$ (degree of linear polarization), P_{22}/P_{11}, P_{33}/P_{11}, P_{43}/P_{11}, and P_{44}/P_{11} as functions of the scattering angle for the three ice crystal models and two spectral bands. The element P_{11} is the phase function. For the regular column $L/D = 120/60$ (μm), P_{11} displays a strong 22° halo peak caused by two refractions through a 60° prism angle, a 46° halo peak due to two refractions through a 90° prism angle, and a third peak between 150° and 160° resulting from the superposition of rays subject to one and two internal reflections. A less prominent secondary peak also occurs at around 170°, formed by the superposition of rays subject to higher-order reflections. For the irregular column $L/D = 120/60$ (μm), the magnitude of the 22° halo peak is reduced and the other peaks disappear, because the added surface roughness yields a broad distribution of prism angles rather than only having discrete values at 60° and 90°. For the plate, the peaks formed by prism refraction and reflection effects are notable but less prominent than those for the regular column.

For the regular column, there are two local minima of $-P_{12}/P_{11}$ around 22° and 46°, corresponding to the halo features shown in the plot of P_{11}. Between 110° and 160°, there is also a broad peak with magnitude ranging from 0.1 to 0.2 for the 0.865-μm band, and from 0.1 to 0.3 for the 2.25-μm band due to combined effects of external and internal reflections. Externally reflected rays with positive degree of linear polarization would have caused a peak at around 80° with magnitude approaching 1 between 60° and 160°. Because of a large number of internally reflected rays with negative degree of linear polarization for scattering angles less than 110°, the values of $-P_{12}/P_{11}$ are reduced to less than 0.1 for scattering angles less than 110°, resulting in the broad peak between 110° and 160°. For regular plates, the broad peak between 110° and 160° remains, but the values of $-P_{12}/P_{11}$ are larger than those for the regular column due to a smaller number of internally reflected rays for a scattering angle less than 110°. This diagram also shows that for $120° < \Theta < 150°$, $-P_{12}/P_{11}$ depends on the regularity (or smoothness) of the ice crystal surface, while for $60° < \Theta < 110°$, $-P_{12}/P_{11}$ is sensitive to the ice crystal aspect ratio (plate or column type). It appears evident that the angular distribution of the degree of linear polarization ($-P_{12}/P_{11}$), and hence r_Q exhibits the shape information, which is conducive for the reliable inference of the ice crystal shape factor.

The element P_{22}/P_{11} is nearly 1 in the forward-scattering direction. It decreases with increasing scattering angle due to the nonsphericity of the ice crystal and the relative strength of external and internal reflections. For a spherical particle or for the case where only externally reflected rays are considered, P_{22}/P_{11} would be 1. As mentioned above for the regular column, a large number of internally reflected rays interfere with the externally reflected rays at scattering angles less than 110°, so that P_{22}/P_{11} is smaller than 1. For the regular plate, P_{22}/P_{11} is closer to 1 than for the regular column, because the strength of externally reflected rays dominates other rays. Oscillations of P_{22}/P_{11} due to various reflection components for the regular column are smoothed out by the surface roughness for the irregular column, so that the curve becomes smooth.

The element P_{33}/P_{11} decreases with increasing scattering angle. It crosses over the zero line at an intermediate scattering angle (Θ_{33}) because of the phase-shift effect. If only the external reflection is considered, the crossover angle Θ_{33} would be around 80°. However, with the superposition of internally reflected rays, Θ_{33} is shifted between 100° and 120°. For the regular plate, P_{33}/P_{11} is smaller than for the regular column because the strength of externally reflected rays dominates internally reflected rays. The curve of P_{33}/P_{11} for irregular columns is smoother than that for regular columns

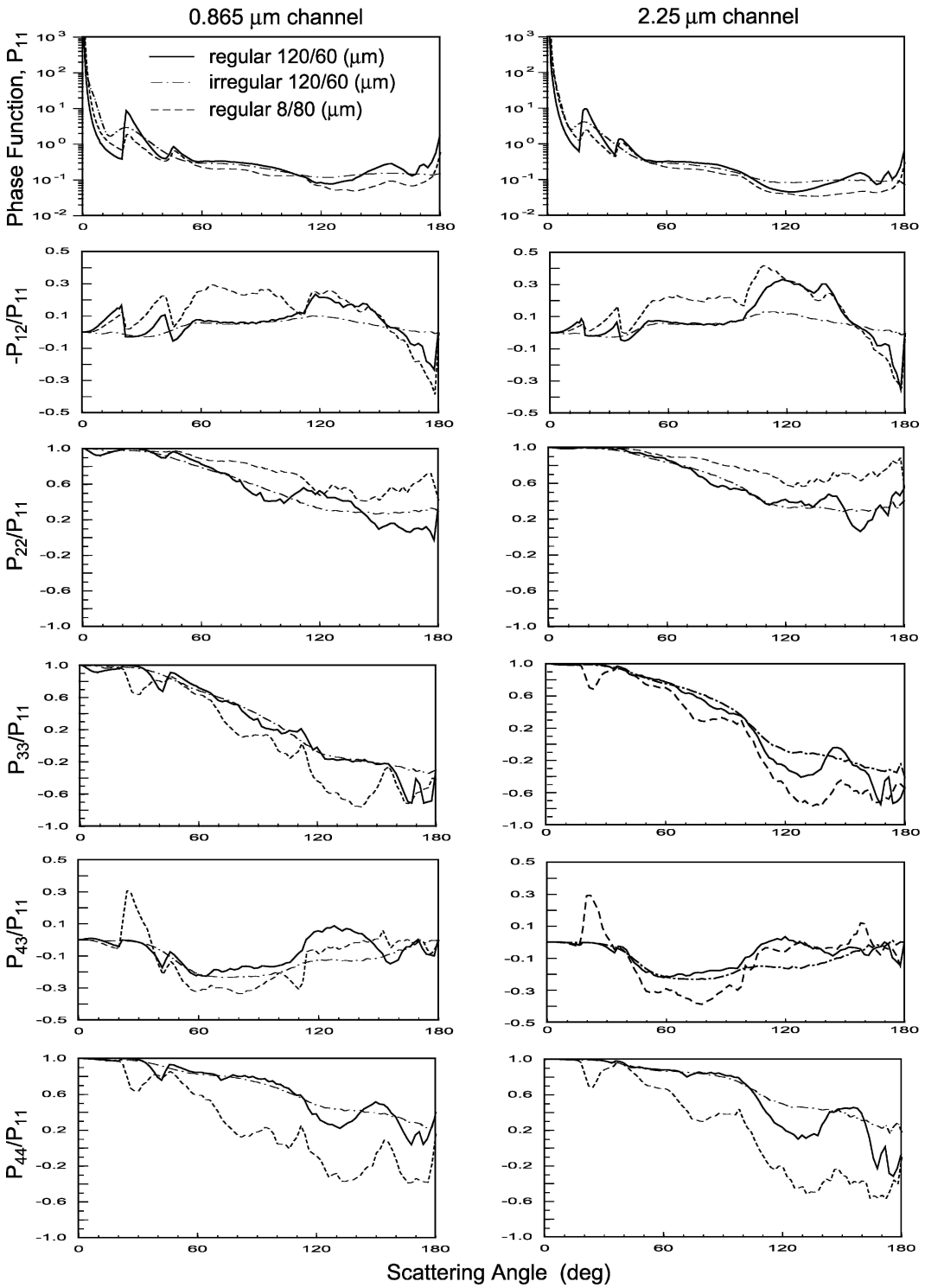

FIG. 2. Phase-matrix elements P_{11}, $-P_{12}/P_{11}$, P_{22}/P_{11}, P_{33}/P_{11}, P_{43}/P_{11}, and P_{44}/P_{11}, for the 0.865- and 2.25-μm bands. Results are shown for three combinations of ice crystal shape and size.

due to the broad angular distribution of scattered rays. The element P_{43}/P_{11} ranges between -0.3 and 0.3. There is a peak near 22° for the regular plate. This peak results from the total internal reflection. The curve of P_{43}/P_{11} for irregular column is smoother than for regular column due to the broad angular distribution of rays caused by the surface roughness of the irregular column. The element P_{44}/P_{11} is always larger than or equal to the element P_{33}/P_{11}. Similar to the behavior of P_{22}/P_{11}, P_{44}/P_{11} is equal to P_{33}/P_{11} for a spherical particle or for the case where only externally reflected rays are considered. Thus, the differences between P_{44}/P_{11} and P_{33}/P_{11} result from the nonsphericity of the scattering particle.

Overall, each of the six elements for the two bands shows some sensitivity toward ice crystal shape, size, and surface roughness due to the various optical effects. The diagonal elements (P_{ii}, $i = 1, 4$) display larger sensitivity toward ice crystal shape and size in the backscattering range than in the forward-scattering range. This behavior is conducive for the remote sensing of ice crystal shape and size parameters, because polarimetric sensors on board aircraft and satellites mostly measure radiation in the backscattering direction during midday flight or overpass. The surface roughness only smoothes out the peaks of the diagonal elements. The off-diagonal elements (P_{12} and P_{43}) in the backscattering direction are more sensitive to particle surface roughness than to shape and size.

b. Polarization parameters

Figures 3a,b for 0.865 and 2.25 μm, respectively, show r_I, r_Q, and polarization ratio (P), versus viewing zenith angle for three ice crystal mean effective sizes (D_e = 24, 42, and 124 μm) and three optical depths (τ = 0.25, 2, and 10). The three ice crystal mean effective sizes are derived based on measured composite ice crystal size distribution (Ou et al. 2003), assuming randomly oriented regular columns. The sun-sensor configuration is consistent with the 17 April EUCREX morning case reported by Chepfer et al. (1998). The solar zenith angle is fixed at 55.3°. The relative azimuthal angle is either 0° or 180°, because the sun is directly behind the aircraft. The viewing zenith angle is the viewing angle relative to satellite nadir, and its negative and positive signs correspond to the backward and forward directions, respectively. The surface albedo is assumed to be zero. The parameter r_U is invariably zero for this sun-sensor geometry and is not shown.

The bidirectional reflectance r_I increases with increasing optical depth, but decreases with increasing ice crystal size. The 0.865-μm r_I is more sensitive to optical depth, while the 2.25-μm r_I is more sensitive to ice crystal size. The prominent peak at $\theta \approx 57°$ for both bands results from the ice glory peak in the backscattering direction. The parameter r_Q for both bands is more sensitive to optical depth in the backward-viewing direction than in the forward-viewing direction. The minima at $\theta \approx 57°$ in r_Q results from a minimum in the degree of linear polarization $-P_{12}/P_{11}$ at a scattering angle $\Theta = 178°$ (as shown in Fig. 2), and its magnitude increases with the optical depth, but decreases with larger particle size, and is larger for the 0.865-μm band. For the present case, P is actually the absolute value of the ratio of r_Q to r_I since r_U is zero. Its magnitude decreases with increasing optical depth, but increases with the ice crystal size in the backscattering direction. The peak near 10° is caused by the minimum value of r_I at that angle, and the peak at ~57° is due to the combined effect of the peak in r_I and the minima in r_Q. In addition, the polarization ratio is not sensitive to the ice crystal size for the viewing angles greater than 30° corresponding to the scattering angles greater than 156°.

c. Verification and application of the retrieval scheme

To verify the retrieval scheme, and to assess effects of radiometric and polarimetric uncertainties on the retrieval accuracy, we perform three types of synthetic tests: algorithm accuracy, radiometric accuracy, and polarimetric accuracy. For the algorithm accuracy test, simulated polarization parameters without perturbation for all combinations of reference effective particle sizes and optical depths are treated as measured data and input into the retrieval program. Subsequently, radiometric error (5%) and polarimetric error (0.2%) are separately added to the simulated polarization parameters to perform the retrieval. To explore the advantage of increased scattering angle information, retrievals using multiple viewing zenith angles [J = 1–4 in Eq. (17)] have been performed.

The algorithm accuracy test yields zero errors for all combination of reference effective particle sizes and optical depths and for all combinations of viewing zenith angles, implying that the algorithm using the steepest-descent method is highly accurate and numerically stable. Nearly zero retrieval errors are also obtained from the polarimetric accuracy test, indicating errors in the polarization ratio based on representative instrument design would not deteriorate the retrieval performance. On the other hand, the radiometric accuracy test yields errors of 0–0.7 μm in retrieved effective particle size, and errors of 0–0.8 in retrieved optical depth.

To illustrate the effectiveness of our retrieval scheme, we construct a 2D correlation diagram between the polarization ratio, P, and the bidirectional

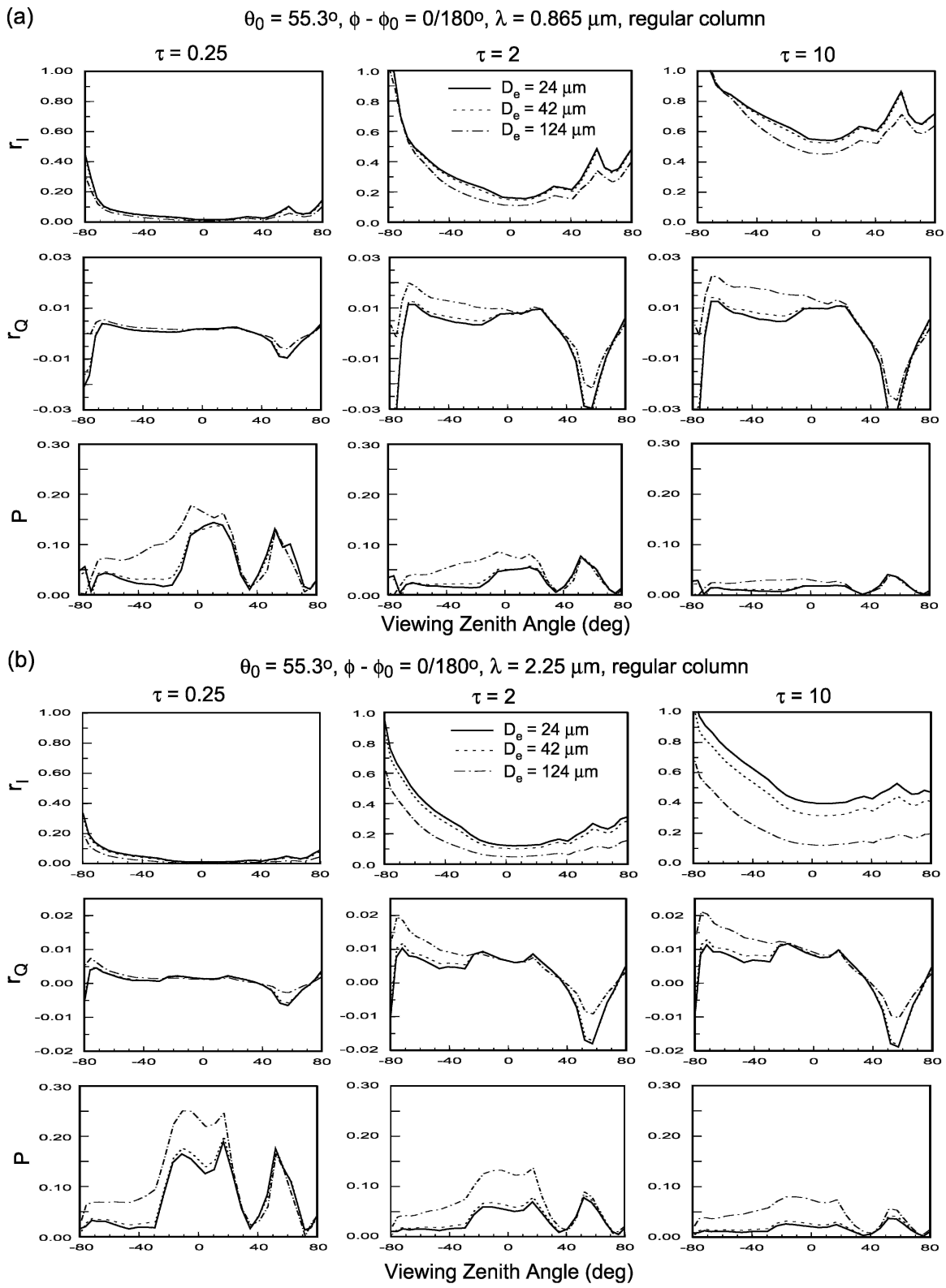

FIG. 3. Values of r_I and r_Q vs viewing zenith angle for three ice crystal mean effective sizes and three optical depths for the (a) 0.865- and (b) 2.25-μm polarization ratio (P).

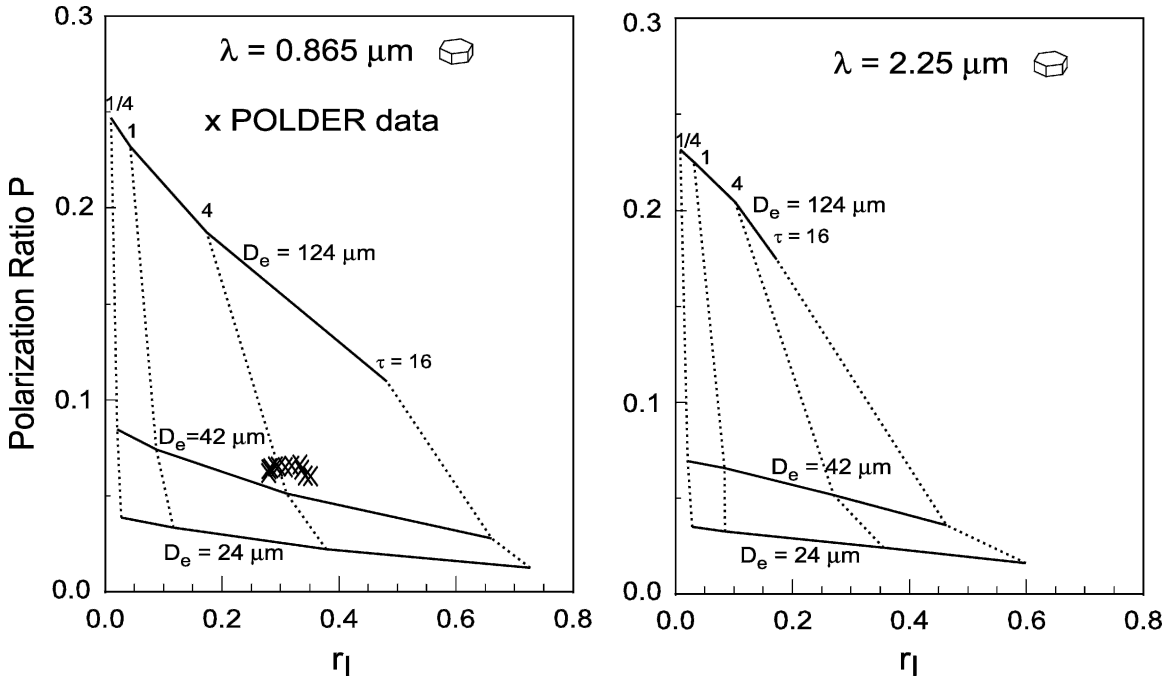

FIG. 4. Two-dimensional polarization/reflectance correlation diagram in terms of the mean effective size D_e and the optical depth τ for two near-IR wavelengths of 0.865 and 2.25 μm using ice plates in the calculation for a solar zenith angle of 55.3°, a viewing zenith angle of −30°, and a surface albedo of 0.0.

reflectance, r_I, for the previously defined wavelengths, ice crystal shapes, and sizes. In Fig. 4, we present results for the plate case for a solar zenith angle of 55.3°, a viewing zenith angle of −30° corresponding to a scattering angle of 95°, and a surface albedo of 0.0. The solid lines represent constant ice crystal size in terms of the mean effective width (size), D_e (Ou et al. 2003) while the dashed lines represent constant optical depth. There is a strong sensitivity of polarization ratio to effective ice crystal size. Our previous work (Takano and Liou 1989a,b) illustrates that P increases with decreasing length–width ratio, L/D (L is the length and D is the width) for a range of scattering angles from 60° to 120°. The mean effective size D_e is inversely proportional to L/D so that if D_e increases, the polarization ratio increases.

Also displayed in Fig. 4a are the correlation of 0.865-μm P and r_I derived from the POLDER data obtained in the morning on 17 April 1994 over Brittany, France, during EUCREX. Since POLDER does not have a near-IR polarization channel (Deschamps et al. 1994), the simulated 2.25-μm correlation of P and r_I cannot be applied to POLDER data, and there is no overlapping measurements in Fig. 4b. These measurements were provided by Chepfer et al. (1998) and presented in Fig. 1 (Liou and Takano 2002). The data were taken over the thicker portion of a single layer of cirrus located between 8 and 10 km. The viewing angles for the data are between −25° and −35°, which correspond to scattering angles of 100° and 90°, respectively. Application of these data to the retrieval scheme leads to an optical depth of about 4 and a mean effective width of about 45 μm. Processing of in situ measurements during EUCREX leads to the effective radius of 24 μm, or an effective diameter of about 48 μm (Sauvage et al. 1999). This value is close to the 45 μm derived from Fig. 4.

Based on the results shown in Fig. 3, we have also constructed a similar 2D correlation of P and r_I for a regular column. Application of the same 0.865-μm POLDER data to this new correlation leads to an optical depth of about 4 and a mean effective width of about 24 μm. Use of the regular column and plate yields similar optical depth, because r_I as a function of optical depth varies little from regular column to plate. The mean effective width for regular column differs from that for plate by about 21 μm, because the P as a function of size is quite sensitive to shape variation. Overall, these results show that multiangle measurements are required to reliably determine ice crystal shape, optical depth, and mean effective width.

4. Concluding remarks

In this paper, we present a conceptual approach toward the remote sensing of cirrus cloud particle size

and optical depth using the degree of polarization and polarized reflectances associated with the first three Stokes parameters I, Q, and U for the 0.865- and 2.25-μm wavelengths. For the purpose of simulating the clear and cloudy polarization parameters and performing a sensitivity study of the retrieval algorithms, we have developed a vector line-by-line equivalent radiative transfer program including the full Stokes parameters based on the adding method. Single-scattering parameters and phase-matrix elements were computed for randomly oriented hexagonal ice crystals. The retrieval algorithm employs the steepest-descent method in the form of a series of numerical iteration procedures to search for cloud properties with polarization parameters that best match the measured polarization parameters.

Sensitivity studies were performed to investigate the behavior of phase-matrix elements as functions of the scattering angle for three ice crystal size–shape combinations. Overall, each phase-matrix element shows sensitivity toward ice crystal shape, size, and surface roughness due to various optical effects. In particular, the diagonal elements display larger sensitivity toward ice crystal shape and size in the backscattering range than in the forward-scattering range. We also investigated the variation of polarization parameters with the viewing zenith angle. We found that polarization parameters are sensitive to optical depth for all viewing zenith angles. The parameter r_Q has a strong sensitivity to particle size in the backscattering direction, while the parameter P varies significantly with particle size in the side-scattering and backscattering directions. Synthetic retrievals reveal that the retrieval algorithm is numerically stable and precise, and the polarimetric and radiometric error sources cause reasonably small retrieval errors. Finally, an example illustrating the applicability of the present retrieval algorithm to airborne POLDER data has been presented. Reasonable values of cirrus cloud particle size and optical depth have been obtained.

Acknowledgments. This research was supported in part by Northrop-Grumman Space Technology Contracts 95031DDM3S and 97904DDM3S, and by NSF Grants ATM-9907924 and ATM-0331550. POLDER polarimetric data were provided by H. Chepfer.

REFERENCES

Bréon, F.-M., and B. Dubrulle, 2004: Horizontally oriented plates in clouds. *J. Atmos. Sci.,* **61,** 2888–2898.

Cai, Q. M., and K. N. Liou, 1982: Theory of polarized light scattering by hexagonal ice crystals. *Appl. Opt.,* **21,** 3569–3580.

Cairns, B., L. D. Travis, and E. E. Russell, 1999: Research Scanning Polarimeter: Calibration and ground-based measurements. *Proc. SPIE,* **3754,** 186–197.

Chepfer, H., G. Brogniez, and Y. Fuquart, 1998: Cirrus clouds' microphysical properties deduced from POLDER observations. *J. Quant. Spectrosc. Radiat. Transfer,* **60,** 375–390.

——, ——, P. Goloub, F. M. Brèon, and P. H. Flamant, 1999a: Observations of horizontally oriented ice crystals in cirrus clouds with POLDER-1/ADEOS-1. *J. Quant. Spectrosc. Radiat. Transfer,* **63,** 521–543.

——, ——, L. Sauvage, P. H. Flamant, V. Trouillet, and J. Pelon, 1999b: Remote sensing of cirrus radiative parameters during EUCREX'94. Case study of 17 April 1994. Part II: Microphysical models. *Mon. Wea. Rev.,* **127,** 504–519.

Coffeen, D. L., 1979: Polarization and scattering characteristics in the atmosphere of Earth, Venus, and Jupiter. *J. Opt. Soc. Amer.,* **69,** 1051–1064.

Deschamps, P.-Y., F.-M. Bréon, M. Leroy, A. Podaire, A. Bricaud, J.-C. Biriez, and G. Sèze, 1994: The POLDER Mission: Instrument characteristics and scientific objectives. *IEEE Trans. Geosci. Remote Sens.,* **32,** 598–615.

Goloub, P., J. L. Deuzé, M. Herman, and Y. Fouquart, 1994: Analysis of the POLDER polarization measurements performed over cloud covers. *IEEE Trans. Geosci. Remote Sens.,* **32,** 78–88.

Hovenier, J. W., 1969: Symmetry relationships for scattering of polarized light in a slab of randomly oriented particles. *J. Atmos. Sci.,* **26,** 488–499.

King, M. D., S. C. Tsay, S. E. Platnick, M. Wang, and K. N. Liou, 1997: Cloud retrieval algorithm for MODIS: Optical thickness, effective particle radius, and thermodynamic phase. MODIS algorithm theoretical basis document ATBD, MOD-05, 83 pp.

Liou, K. N., 2002: *An Introduction to Atmospheric Radiation.* 2d ed. Academic Press, 583 pp.

——, and Y. Takano, 1994: Light scattering by nonspherical particles: Remote sensing and climatic implications. *Atmos. Res.,* **31,** 271–298.

——, and ——, 2002: Interpretation of cirrus cloud polarization measurements from radiative transfer theory. *Geophys. Res. Lett.,* **29,** 1313, doi:10.1029/2001GL014613.

——, Q. M. Cai, J. B. Pollack, and J. N. Cuzzi, 1983: Light scattering by randomly oriented cubes and parallelpipeds. *Appl. Opt.,* **22,** 3001–3008.

Lynch, D. K., K. Sassen, D. O. Starr, and G. Stephens, Eds., 2002: *Cirrus.* Oxford University Press, 480 pp.

Mace, G. G., T. P. Ackerman, E. E. Clothiaux, and B. A. Albrecht, 1997: A study of composite cirrus morphology using data from a 94 GHz radar and correlations with temperatures and large-scale motion. *J. Geophys. Res.,* **102,** 13 581–13 593.

Macke, A., and M. I. Mishchenko, 1996: Applicability of regular particle shapes in light scattering calculations for atmospheric ice particles. *Appl. Opt.,* **35,** 4291–4296.

Masuda, K., H. Ishimoto, and T. Takashima, 2002: Retrieval of cirrus optical thickness and ice-shape information using total and polarized reflectance from satellite measurements. *J. Quant. Spectrosc. Radiat. Transfer,* **75,** 39–51.

Minnis, P., D. P. Garber, D. F. Young, R. F. Arduini, and Y. Takano, 1998: Parameterizations of reflectance and effective emittance for satellite remote sensing of cloud properties. *J. Atmos. Sci.,* **55,** 3313–3339.

Mishchenko, M. I., W. B. Rossow, A. Macke, and A. Lacis, 1996: Sensitivity of cirrus cloud albedo, bidirectional reflectance

and optical thickness retrieval accuracy to ice-particle shape. *J. Geophys. Res.,* **101,** 16 973–16 989.

Nadal, F., and F.-M. Bréon, 1999: Parameterization of surface polarized reflectance derived from POLDER spaceborne measurements. *IEEE Trans. Geosci. Remote Sens.,* **37,** 1709–1718.

Noel, V., and H. Chepfer, 2004: Study of ice crystal orientation in cirrus clouds based on satellite polarized radiance measurements. *J. Atmos. Sci.,* **61,** 2073–2081.

Ou, S. C., K. N. Liou, M. D. King, and S. C. Tsay, 1999: Remote sensing of cirrus cloud parameters based on a 0.63–3.7 μm radiance correlation technique applied to AVHRR data. *Geophys. Res. Lett.,* **26,** 2437–2440.

——, Y. Takano, K. N. Liou, G. J. Higgins, A. George, and R. Slonaker, 2003: Remote sensing of cirrus cloud optical thickness and effective particle size for the National Polar-orbiting Operational Environmental Satellite System Visible/Infrared Imager Radiometer Suite: Sensitivity to instrument noise and uncertainties in environmental parameters. *Appl. Opt.,* **42,** 7202–7214.

Rolland, P., and K. N. Liou, 2001: Surface variability effects on the remote sensing of thin cirrus optical and microphysical properties. *J. Geophys. Res.,* **106,** 22 965–22 977.

——, ——, M. D. King, S. C. Tsay, and G. M. McFarquhar, 2000: Remote sensing of optical and microphysical properties of cirrus clouds using MODIS channels: Methodology and sensitivity to assumptions. *J. Geophys. Res.,* **105,** 11 721–11 738.

Sauvage, L., H. Chepfer, V. Trouillet, P. H. Flamant, G. Brogniez, J. Pelon, and F. Albers, 1999: Remote sensing of cirrus radiative parameters during EUCREX'94. Case study of 17 April 1994. Part I: Observations. *Mon. Wea. Rev.,* **127,** 486–503.

Takano, Y., and K. N. Liou, 1989a: Solar radiative transfer in cirrus clouds. Part I: Single-scattering and optical properties of hexagonal ice crystals. *J. Atmos. Sci.,* **46,** 3–19.

——, and ——, 1989b: Solar radiative transfer in cirrus clouds. Part II: Theory and computation of multiple scattering in an anisotropic medium. *J. Atmos. Sci.,* **46,** 20–36.

——, and ——, 1993: Transfer of polarized infrared radiation in optically anisotropic media: Application to horizontally oriented ice crystals. *J. Opt. Soc. Amer.,* **10,** 1243–1256.

——, and ——, 1995: Radiative transfer in cirrus clouds. Part III: Light scattering by irregular ice crystals. *J. Atmos. Sci.,* **52,** 818–837.

Tarantola, A., 1987: *Inverse Problem Theory.* Elsevier Science, 613 pp.

Wylie, D., and W. P. Menzel, 1999: Eight years of global high cloud statistics using HIRS. *J. Climate,* **12,** 170–184.

Yang, P., and Q. M. Cai, 1991: Scattering phase matrices of ice crystals with hexagonal prism and triangular pyramid form—A vector ray tracing method. *Acta Meteor. Sin.,* **5,** 515–526.

——, and K. N. Liou, 1998: Single-scattering properties of complex ice crystals in terrestrial atmosphere. *Contrib. Atmos. Phys.,* **71,** 223–248.